Solute trapping in directional solidification at high speed: A one-dimensional study with the phase-field model

M. Conti
Dipartimento di Matematica e Fisica, Università di Camerino, 62032 Camerino, Italy
(Received 3 March 1997)

The rapid solidification of a binary alloy, directed by a moving temperature field, is studied with the phase-field model. Unlike previous findings solute segregation at the interface can be properly described through the usual formulation of the model, without concentration gradient corrections. The governing equations of the model are numerically solved to determine the interface temperature and the solute concentration field as a function of the interface velocity v. The partition coefficient $k(v)$ is monotonically increasing towards unity at large growth rates; the interface temperature T_I first rises, then falls with increasing v. The results show good agreement with the predictions of the continuous growth model of Aziz and Boettinger [M. J. Aziz and W. J. Boettinger, Acta Metall. Mater. **42**, 527 (1994)]. [S1063-651X(97)12408-4]

PACS number(s): 64.70.Dv, 68.10.Gw, 81.30.Bx, 82.65.Dp

Rapid solidification of binary alloys is addressed through sharp interface or phase-field models. Sharp interface models [1,2] utilize the diffusion equation to describe the transport of heat and solute through the bulk phases; the interface boundary conditions reflect two different constraints: (i) the energy and solute conservation across the moving front, and (ii) constitutive laws that relate the local interface conditions (concentration c and temperature T) to the front velocity v. Point (ii) requires a separate modellization of the interface kinetics on a microscopic scale, and was addressed by Aziz [3], Aziz and Kaplan [4] and Aziz and Boettinger [5] within the continuous growth model (CGM). They pointed out that the solute redistribution across the solid-liquid interface is driven by a diffusional mechanism characterized by a velocity scale $v_d \sim D/a$, where D is the interface solute diffusivity and a is a length representative of the interface thickness; as the front velocity becomes of the order of v_d this mechanism becomes less effective and the partition coefficient $k(v)$ (i.e., the ratio c_s/c_l of solute concentration in the growing solid to that in the liquid at the interface) deviates from the equilibrium value k_e, increasing towards unity at large growth rates. This phenomenon, well known in rapid solidification experiments, is termed ''solute trapping.''

Within the phase-field model (PFM), a phase field $\phi(x,t)$ characterizes the phase of the system at each point; a free-energy (or entropy) functional, depending on ϕ, T, c and including gradient correction terms (generally for ϕ alone) is then extremized in respect to these variables, to derive the dynamic equations for the process. Wheeler, Boettinger, and McFadden [6] were the first to apply the PFM to alloy solidification, in the isothermal limit. They started from a free-energy functional including a $(\nabla\phi)^2$ term and conducted an asymptotic analysis of the governing equations for a vanishing small interface thickness; the partition coefficient k resulted in a decreasing function of the front velocity, and the authors concluded that the model was unable to predict solute trapping. The same conclusion could be drawn from the sharp interface limit of a slightly different version of the model proposed by Caginalp and Jones [7]. In a successive study Wheeler, Boettinger, and McFadden [8] recovered the correct dependence $k(v)$ through the inclusion in the free-energy functional of a $(\nabla c)^2$ term, acting to oppose the contraction of the solute profile at large velocities.

It is the aim of the present study to show that the phase-field model, in the more natural formulation given by [6,7], contains all the ingredients for a proper description of solute trapping. A large but finite diffusional velocity v_d for the interfacial solute redistribution is naturally embedded in the governing equations; it is precisely the sharp interface limit taken in [6,7] that, pushing v_d towards infinity, precluded the possibility of solute trapping prediction.

The solidification process, driven by a moving temperature field, will be simulated in one dimension. The system is an ideal binary solution with constituents A (solvent) and B (solute). Initially a solid ($x<x_0$) and a liquid ($x>x_0$) region are separated by an interface at temperature T_I. The solute concentration in the solid and liquid phases is fixed to the equilibrium values at T_I. Then the temperature field, characterized by a positive uniform gradient G, is pulled towards the positive x direction at constant velocity V_0, and the solidification front follows the advancing isotherms. This arrangement is well representative of standard directional solidification experiments, when heat diffusion is much faster than solute diffusion, and allows one to decouple the temperature from the concentration and the phase fields.

The problem will be treated in nondimensional form, scaling lengths to some reference length ξ and time to ξ^2/D_l, D_l being the solute diffusivity in the liquid phase. A nondimensional temperature is defined as $u=C(T-T_m^A)/L^A$, where T_m^A and L^A are the melting temperature and the latent heat of the pure solvent; C is the specific heat for which we assume equal values for both solvent and solute, in both phases. The model is presented in full details in [6,9,10]; in the limit $(T-T_I) \ll T_I$ the governing equations become

$$\frac{\partial\phi}{\partial t} = [(1-c)n+c]m\nabla^2\phi - [(1-c)n+c]m \times \left\{ (1-c)\left[\frac{1}{\epsilon^{A2}} \frac{dg(\phi)}{d\phi} - \frac{\alpha^A u}{\epsilon^A} \frac{dp(\phi)}{d\phi} \right] + c\left[\frac{1}{\epsilon^{B2}} \frac{dg(\phi)}{d\phi} - \frac{\alpha^B(u+u^*)}{\epsilon^B \tilde{L}} \frac{dp(\phi)}{d\phi} \right] \right\}, \quad (1)$$

$$\frac{\partial c}{\partial t}=\nabla\cdot\{\lambda(\phi)\nabla c-c(1-c)\lambda(\phi)[H^A(\phi,T)$$

$$-H^B(\phi,T)]\nabla\phi-c(1-c)\lambda(\phi)\Gamma(\phi,T)\nabla u\},\quad(2)$$

$$\frac{\partial u}{\partial t}=-V_0\frac{\partial u}{\partial x}=-V_0G.\quad(3)$$

In Eq. (1) $g(\phi)=(1/4)\phi^2(1-\phi)^2$ is a symmetric double-well potential with equal minima at $\phi=0$ and $\phi=1$; $p(\phi)$ is a monotonically increasing function of ϕ from $p(0)=0$ in the solid to $p(1)=1$ in the liquid; with the choice $p(\phi)=\phi^3(10-15\phi+6\phi^2)$ the bulk solid and liquid are described by $\phi=0$ and $\phi=1$, respectively, for every value of temperature.

In Eq. (2) the function $H^A(\phi,T)$ is given by

$$H^A(\phi,T)=W^A\frac{dg(\phi)}{d\phi}-\frac{v_m}{R}\frac{dp(\phi)}{d\phi}L^A\frac{T-T_m^A}{TT_m^A},\quad(4)$$

where v_m is the molar volume and R is the gas constant; a similar expression holds for $H^B(\phi,T)$. The function $\Gamma(\phi,T)$ is given by

$$\Gamma(\phi,T)=-\frac{p(\phi)}{T^2}\frac{v_m}{R}\frac{L^A}{C}(L^A-L^B)\quad(5)$$

and $\lambda(\phi)$, defined as

$$\lambda(\phi)=\frac{D_s}{D_l}+p(\phi)\left(1-\frac{D_s}{D_l}\right)\quad(6)$$

describes the smooth transition of the bulk solute diffusivity from D_s (in the solid) to D_l (in the liquid).

The model parameters $\alpha^{A,B},\epsilon^{A,B},W^{A,B},m,n,\tilde{L},u^*$ were associated to the physical properties of the alloy components by Warren and Boettinger [10]; below only the results are synthesized:

$$\alpha^{A,B}=\frac{L^{A,B}}{C\overline{T_I}}\frac{\xi L^{A,B}}{6\sqrt{2}\sigma^{A,B}},\quad\epsilon^{A,B}=\frac{h^{A,B}}{\xi},$$

$$W^{A,B}=\frac{v_m}{R}\frac{12\sigma^{A,B}}{\sqrt{2}T_m^{A,B}h^{A,B}},\quad m=\frac{\beta^B\sigma^BT_m^B}{D_lL^B},$$

$$n=\frac{\beta^A\sigma^AT_m^AL^B}{\beta^B\sigma^BT_m^BL^A},\quad u^*=\frac{C(T_m^A-T_m^B)}{L^A},$$

$$\tilde{L}=\frac{L^B}{L^A},\quad(7)$$

where $\sigma^{A,B}$ is the surface tension of pure A or B; $\beta^{A,B}$ is the kinetic undercooling coefficient, that relates the interface undercooling to the interface velocity through $v=\beta^{A,B}(T_m^{A,B}-T)$. In the phase-field model for a pure substance the interface thickness is a free and independent parameter that has been indicated in Eq. (7) through $h^{A,B}$. It can be shown [10] that a model constraint imposes $\epsilon^A\sqrt{W^A}=\epsilon^B\sqrt{W^B}$; then the condition is forced:

TABLE I. Material parameters for the Ni-Cu alloy.

	Nickel	Copper
T_m (K)	1728	1358
L (J/cm^3)	2350	1728
v_m (cm^3/mol)[a]	7.0	7.8
σ (J/cm^2)	3.7×10^{-5}	2.8×10^{-5}
β (cm/K s)[b]	160	198
D_l (cm^2/s)	10^{-5}	10^{-5}

[a]An average value of 7.4 will be taken.
[b]From the estimation of Willnecker *et al.* [12].

$$h^B/h^A=\sigma^AT_m^B/\sigma^BT_m^A.\quad(8)$$

To estimate the above parameters we referred to the termophysical properties of nickel (solvent) and copper (solute), summarized in Table I. The length scale was fixed at $\xi=2.1\times10^{-4}$ cm; a realistic value of h^A was selected as $h^A=1.68\times10^{-7}$ cm. With this choice it results in $\alpha^AT_I/T_m^A=395.62$, $\alpha^B\overline{T_I}/T_m^B=347.28$, $\epsilon^A=8.00\times10^{-4}$, $\epsilon^B=8.02\times10^{-4}$, $W^A=0.965$, $W^B=0.961$, $\tilde{L}=0.735$, $m=350$, $n=1.01$. The nondimensional temperature gradient was fixed at $G=2.3$.

The evolution of Eqs. (1)–(3) has been considered in one spatial dimension, in the domain $0\leqslant x\leqslant x_m$ with x_m large enough to prevent finite-size effects. Fluxless boundary conditions for ϕ,c and transparent conditions for u were imposed at the domain's walls.

To discretize the equations second order in space and first order in time, finite-difference approximations were utilized. Then, an explicit scheme was employed to advance the solution forward in time. To ensure an accurate resolution of both the phase field and concentration profiles, the grid spacing was selected as $\Delta x=0.5\tilde{\epsilon}^A$; a time step $\Delta t=2.0\times10^{-10}$ was required for numerical stability. Except for temperatures, dimensionless units will be used to illustrate the numerical results.

The initial concentration of the alloy is set to $c_{-\infty}=0.056\,09$ for the solid phase ($x<x_0$; $\phi=0$) and $c_{+\infty}=0.070\,68$ for the liquid phase ($x>x_0$; $\phi=1$). This corresponds to an equilibrium temperature $T_I=1706.06$ K. Then the initial temperature profile, defined as

$$T(x,0)=\overline{T_I}+G(x-x_0),\quad(9)$$

is pulled toward the positive x direction with constant velocity V_0. After a transient the solidification front selects a steady interface temperature T_I, following the advancing isotherms with their same velocity, and the solid phase grows with uniform concentration $c_{+\infty}$. The solute segregation on the moving front is evaluated computing the maximum value $c_{\max}$ of $c(x,t)$, that identifies the concentration c_l on the liquid side of the interface. We examined two different cases, with the solute diffusivity in the solid $D_s=D_l$ and the more realistic situation with $D_s=10^{-6}D_l$; we will first analyze the case $D_s=D_l$.

Figure 1 shows, in the (c,T) plane, the portion of the equilibrium phase diagram in which we are interested, computed from the data of Table I. The vertical line corresponds

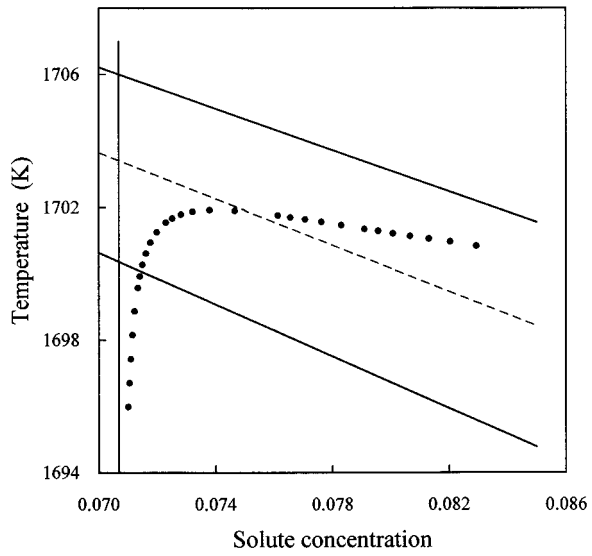

FIG. 1. A portion of the equilibrium phase diagram of the Ni-Cu alloy, computed from the data given in Table I. The vertical line corresponds to the value of $c_{+\infty}$ used in the simulations. The solid dots represent the pairs $(c_{\max},T_I)$ corresponding to the steady solutions found in the present study. The T_0 line is also indicated (dashed curve).

to the value $c_{+\infty}$; it is also indicated on the graph (dashed curve) the T_0 line, i.e., the locus of the pairs c,T for which the Helmholtz free energy of the liquid and solid are equal. The solid dots superimposed on the graph represent the pairs $c_{\max},T_I$ corresponding to the steady solutions found in the numerical simulations; along this path the front velocity is increasing from right to left. It can be observed that, as the velocity increases, the values of $c_{\max}$ approach monotonically the prescribed value $c_{+\infty}=0.070\,68$; this limiting case corresponds to partitionless solidification and complete solute trapping. For small velocity a low undercooling is required for the solidification front to advance, and the interface temperature T_I is only slightly below the equilibrium liquidus temperature; as a consequence T_I increases with v. At higher velocities, when the level of solute trapping nears completion, T_I drops with increasing speed, reflecting an increasing undercooling below the liquidus temperature.

The continuous growth model [3–5] gives the dependence of the partition coefficient on the growth velocity in the form

$$k(v)=\frac{k_e+v/v_d}{1+v/v_d}, \tag{10}$$

where v_d is a characteristic velocity describing the diffusional solute redistribution across the interface; a natural choice is $v_d=D/a$, where D is the interface diffusivity and a is the thickness of the concentration transition layer. In the same model the dependence of the interface temperature on velocity is given, for dilute alloys, by

$$T=T_m^A+\frac{m_l c_{+\infty}}{k}\frac{[1-k+\gamma\ln(k/k_e)]}{1-k_e}-\frac{v}{\beta^A}, \tag{11}$$

where m_l is the slope of the equilibrium liquidus line; the parameter γ is equal to k or equal to unit depending on whether or not solute drag [4,5] is neglected in the dissipation of the free energy that drives solidification.

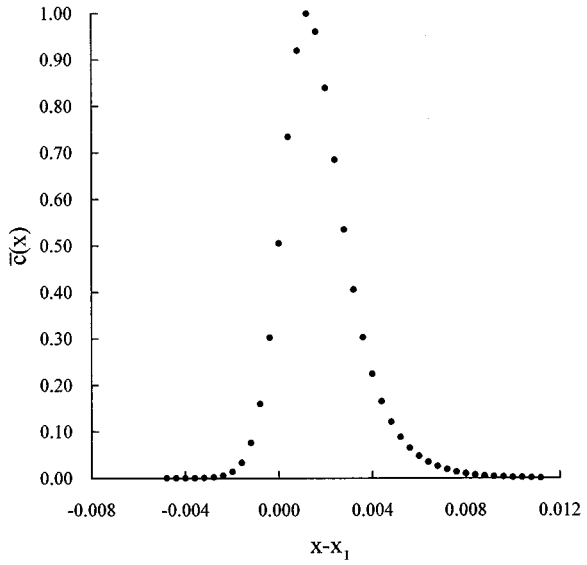

FIG. 2. Normalized concentration profile for $v=800$, $D_s=D_l$; x_I represent the position of the solid-liquid interface, identified at $\phi=0.5$.

Figure 2 shows the solute profile normalized as $\overline{c(x)}=[c(x)-c_{+\infty}]/(c_{\max}-c_{+\infty})$, for $v=800$. We observe that the transition of $\overline{c(x)}$ at the interface takes place within a length that is approximately $a=2\times10^{-3}$; then the diffusional velocity should be $v_d=500$ (here $D=D_l=1$). We utilized this value to compute $k(v)$ through Eq. (10); in Fig. 3 the results are reported, along with the numerical values $c_{\max}/c_{+\infty}$ obtained in the simulations; as it can be observed, the agreement is quite good.

Figure 4 shows the numerical results for the interface temperature as a function of the interface velocity; on the

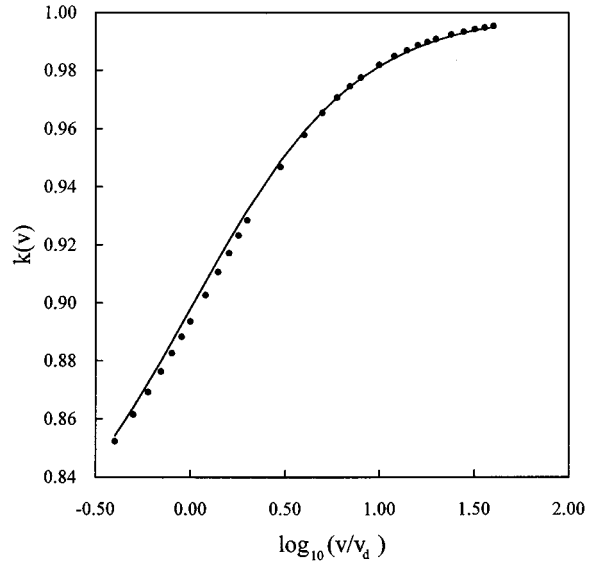

FIG. 3. Partition coefficient $k(v)$ vs the front velocity, for $D_s=D_l$. The solids dots correspond to the values $c_{+\infty}/c_{\max}$ found with the present model; the solid line represents the predictions of the continuous growth model [Eq. (10)].

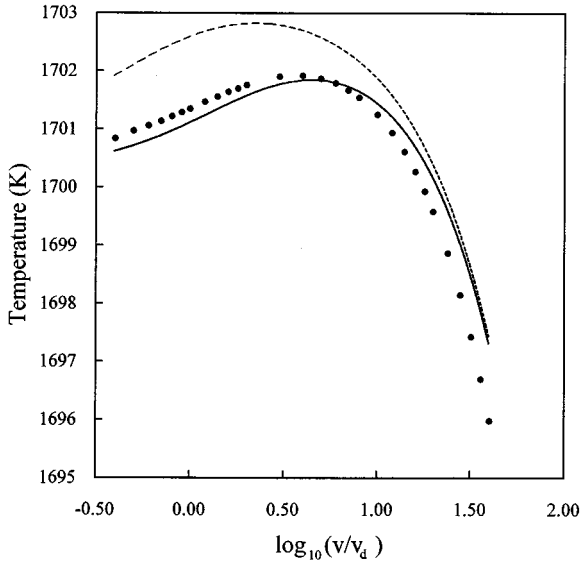

FIG. 4. Interface temperature vs the front velocity, For $D_s = D_l$. The results of the present model (solid dots) are compared with the predictions of the continuous growth model with solute drag (solid line) and without solute drag (dashed line).

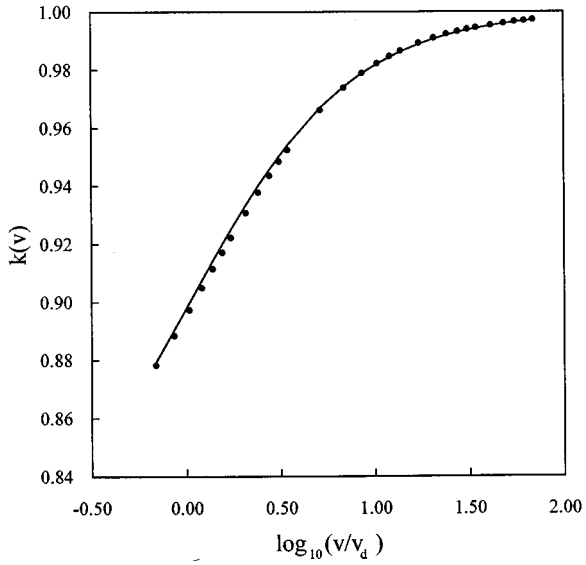

FIG. 5. Partition coefficient $k(v)$ vs the front velocity, for $D_s = 10^{-6} D_l$. The solid dots correspond to the values $c_{+\infty}/c_{\max}$ found with the present model; the solid line represents the predictions of the continuous growth model [Eq. (10)].

same graph we superimposed the curves computed through Eq. (11) with $\gamma = k(v)$ and $\gamma = 1$. The temperatures obtained with the present phase-field model more closely agree with the predictions of the continuous growth model when solute drag is taken into account; as previously argued by Wheeler, Boettinger, and McFadden [8], this is due to the fact that the phase-field model naturally includes surface excesses and their transport during solidification.

When the solute diffusivity in the solid D_s is much lower than D_l, we should expect a reduced effective interface diffusivity and a lower value for v_d. For $D_s = 10^{-6} D_l$ we computed the partition coefficient $k(v)$ as $c_{+\infty}/c_{\max}$, and extracted the value of v_d through Eq. (10) as

$$v_d = v \, \frac{1 - k(v)}{k(v) - k_e}. \tag{12}$$

The best fit of the data gives $v_d = 290$; then, using this value, in Fig. 5 we compare the predictions of the continuous growth model [Eq. (10)] with the present numerical results; here too the agreement is quite satisfactory.

In summary, the phase-field model, in its simpler version including only the ϕ gradient correction, has proved able to predict solute trapping in rapid solidification of binary alloys. This point was not previously recognized, as the asymptotic analysis in the sharp interface limit $\epsilon \to 0$ [6,7] naturally results in an instantaneous re-equilibration of solute and solvent across the moving front, with the diffusional velocity $v_d \sim D/\epsilon$ pushed towards infinity; on the contrary solute trapping, as shown by the continuous growth model, occurs as the front velocity becomes of the order of, or greater than, v_d.

It is worth noting that dropping from the model the c-gradient term, introduced by Wheeler, Boettinger, and McFadden [8] to recover the trapping effect, lowers the order of the differential equation for the solute field, giving a substantially different picture of the process, and allows an easier numerical treatment of the governing equations.

[1] Ch. Charach and B. Zaltzman, Phys. Rev. E **49**, 4322 (1994).
[2] Ch. Charach and Y. Keizman, in *Computational Modelling of Free and Moving Boundaries Problems*, edited by L. C. Wrobel, B. Sarler, and C. A. Brebbia (Computational Mechanics Publications, Southampton, 1995).
[3] M. J. Aziz, J. Appl. Phys. **53**, 1158 (1982).
[4] M. J. Aziz and T. Kaplan, Acta Metall. **36**, 2335 (1988).
[5] M. J. Aziz and W. J. Boettinger, Acta Metall. Mater. **42**, 527 (1994).
[6] A. A. Wheeler, W. J. Boettinger, and G. B. McFadden, Phys. Rev. A **45**, 7424 (1992).
[7] G. Caginalp and J. Jones, Ann. Phys. (N.Y.) **237**, 66 (1995).
[8] A. A. Wheeler, W. J. Boettinger, and G. B. McFadden, Phys. Rev. E **47**, 1893 (1993).
[9] M. Conti (unpublished).
[10] J. A. Warren and W. J. Boettinger, Acta Metall. Mater. **43**, 689 (1995).